International Journal of Science and Research (IJSR)
ISSN: 2319-7064
SJIF (2020): 7.803

Spectropathology of Adrenal Gland is this Possible?

Joanna Dudala, Magdalena Ulatowska Bialas

Abstract: ***Nowadays we can observe increasing attention toward the possibility of the use of FTIR microspectroscopy as a complementary diagnostic method. Research is being conducted to find biomolecular markers of pathological states, including neoplastic changes. To ensure the reliability of the method, wide-range population studies should be done. The best material for studies are fresh, not fixed tissue samples. But in case of rare diseases it is difficult to gather a sufficiently large group of samples. In such case formalin-fixed paraffin-embedded (FFPE) tissue samples are valuable research object. In presented study we tried to find out the biomolecular markers of adrenal gland lesions based on archival FFPE samples using FTIR microspectroscopy. There were three investigated groups: normal adrenocortical tissue, adrenocortical adenoma and adrenocortical carcinoma which is very rare (about 5% of all detected adrenal pathological alterations). We found that the most significant difference is the large content of carbohydrates and nucleic acids in adrenocortical carcinoma. The other difference is rather less significant. Presented study has a preliminary character. They showed the possibility of using the archival FFPE adrenal gland tissue samples but in future it should be considered the application of more sophisticated analysis methods which probably would reveal more difference evidence for classification.***

Keywords: FTIR spectroscopy, adrenal gland, adrenal cortical carcinoma, adrenal cortical adenoma, FFPE samples

1. Introduction

The adrenal glands are paired, small endocrine organs located in the retroperitoneum on the kidney surface. They consist of cortex and medulla which differ in their development and function. The adrenal cortex mainly plays a role in the regulation of water and electrolyte balance (via mineralocorticoid production) and modulates the metabolism of proteins, carbohydrates and fat (via glucocorticoid production). The adrenal medulla is involved in reacting to stress and enabling rapid adaptation to changes in the environment. The adrenal medulla is composed of chromaffin cells which synthesize and secrets catecholamines (mainly epinephrine) [1].

Nowadays, when the image diagnostic methods develop rapidly, and they are easy accessible, the number of detected adrenal gland neoplastic lesions constantly increase. The chirurgical intervention might be done due to oncological (when the imaging examinations suggest the neoplastic lesion) or endocrinological (when the hormonal activity of tumor was confirmed) indications [2, 3]. Although imaging and hormonal studies give a basic knowledge of the tumor nature, the final diagnosis after adrenalectomy is based on the histopthological examination. Classification of adrenal tumors due to their potential malice is based on multivariate evaluation systems based on morphological, clinical and biochemical features, as well as on the evaluation of the tumor proliferative activity using Ki-67 [4, 5]. Nevertheless none of the proposed methods for the differentiation between the benign and malignant tumors is not ideal and fully objective. Therefore it is reasonable to undertake research aimed at finding the complementary methods which could be helpful in differentiating the pathological alterations within the adrenals [6, 7]. The literature reviews shows that it is possible to support diagnosis by comparing the composition of biomolecular and elemental of healthy and pathologically altered tissues. Nowadays the Fourier Transformed Infrared spectroscopy is regarded as a promising complementary diagnostic method [8-14].

The aim of presented study is the attempt to use formalin fixed and paraffin embedded (FFPE) archival adrenal gland tissue samples which constitute a valuable source of clinical material for retrospective studies [15]. It is particularly important in case of studies of the rare samples as it is in case of malignant lesion of adrenal gland. In the range of performed investigations we wanted to answer of two questions. First – is it possible to use deparaffinised adrenal samples for FTIR measurements, second-is it possible to differentiate the pathological states within the adrenal lesion on the basis of obtained results.

2. Material and Methods

2.1. Sample reparation

Investigations were focused at the cortical part of adrenal gland tissue. An archival paraffin embedded blocks of three groups of analysed tissue samples: normal adrenal cortex (N), adrenocortical adenoma (ACA), adrenocortical carcinoma (ACC). All samples were obtained from the Pathomorphology Department, Medical College, Jagiellonian University in Krakow, Poland. The study was approved by the Jagiellonian University Bioethical Committee (KBET/113/B/2014).

From each sample two sections of 6 µm thickness were cut using microtome during the sample preparation. One slice was placed on standard histology glass slide. The second one – for FTIR measurements – was mounted on silver coated sample supports (Low-e MirrIR, Kevely Technologies). To avoid the interference from paraffin on samples IR spectra, they were de-waxed under standard local histological protocol (immersion in xylene (C8H10), in two steps 15 minutes each). All investigated samples were classified by experienced pathologist. They were 21 samples analysed altogether: 5 cases of normal cortex, and 8 cases of adrenocortical adenoma and also 8 incidences of adrenocortical carcinoma.

2.2. FTIR data collection

The measurements were carried out at the Faculty of Physics and Applied Computer Science at AGH University of Science and Technology in Krakow. The measurements were performed using the IR microscope

(Nicolet Continuum-Thermo Scientific) coupled with FTIR spectrometer (Nicolet 8700 – Thermo Scientific). The scientific instrumentation was equipped with ceramic infrared radiation source (the range of 20 ÷ 9600 cm^{-1}) and the MCT detector (mercury cadmium telluride, HgCdTeO2) liquid nitrogen cooled. The samples were analyzed intransflection mode [16] with a beam defined by the aperture 20 µm x 20 µm. The spectra were collected with the OMNIC software (v.8.0) for the wave number range from 800 cm^{-1} to 4000 cm^{-1} with a spectral resolution of 8 cm^{-1} and 150 scans were collected per spectrum (400 scans per background spectrum).

Comparing the microscoping image of the histological specimen and the sample prepared for FTIR measurements 3 to 5 representative areas were chosen for further study. Then 30 to 100 points from each area were manually selected for the FTIR spectroscopic measurements. Great attention was given to this procedure as the points should have been characteristic for the analyzed tissue type (N, ACA and ACC).

2.3. FTIR data processing and analysis

Data processing was performed using the OPUS 7.0 software (Bruker Optics, Ettlingen-Germany). The range of 3800-900 cm^{-1} was separated from all spectra. For general quality comparison the averaged spectra of studied tissue types were prepared. Subsequently they were baseline corrected, using the concave rubber band algorithm (10 iterations and 64 points). Then the offset and vector normalization was applied. It was convenient way to show the main differences between three studied tissue types. Besides, on the basis of the pre-processed spectra, an attempt was made to estimate the area under the main massifs in the range of fingerprints. However it must be remembered that FTIR spectra can be much distorted by several physical phenomena. First of all the baseline can be affected by Mie scattering due to particles of size comparable with the infrared wavelengths (typically between 2.5 µm and 25 µm) as well as the light dispersion from tissue boundaries [17, 18]. The other reported reason for baseline aberrations might arise from substrate effects [19]. Besides, the environmental factors can affect the nature of baseline (the temperature and humidity). To overcome those restrictions, for the quantitative and semi-quantitative analysis, it is recommended to use the second derivative which corrects baseline shift and resolves overlapping bands [17]. In our study this procedure was also applied, the Savitzky-Golay method with 9 points smoothing was used. The second derivative was used to determine the main absorption bands (particularly within the amide I spectral region) of studied sample types as well as to perform the semi-quantitative analysis of the biomolecular composition. The fact that the peak height of the second derivative is proportional to the original peak was used in analysis [17].

The statistical significance of the differences between medians of the analysed parameters for all studied lesions was tested with the non-parametric Mann-Whitney U test at a significance level of 0.05. Non-parametric tests are used for variables which do not fulfill the normal distribution, as in the present analysis. According to the null hypothesis there is no statistically significant difference between groups. It is rejected when $p < 0.05$.

3. Results

The comparison of averaged and baseline corrected spectra for normal cortex (N), adrenocortical adenoma (ACA) and adrenocortical carcinoma (ACC) are shown in Figure 1. The tentative assignments of the band frequencies present in IR spectra measured for tissue samples are listed in Table 1.

Table 1: Tentative assignments of the band frequencies present in IR absorption spectra [17, 20, 21]

Frequency (cm^{-1})	Assignments
~ 3500-3200	ν (O–H): (hydroxyl groups)
~ 3200-3300	ν (N–H): (proteins, amide A)
~ 3080	ν (N–H): (proteins, amide B)
~ 3020-3000	ν (=CH): (olefinic) unsaturated fatty acids, cholesterol esters
~ 2990-2950	ν_{as} (CH_3): (methyl) phospholipids, cholesterol esters, fatty acids
~ 2950-2880	ν_{as} (CH_2): (methylene) phospholipids, long chain fatty acids
~ 2880-2860	ν_s (CH_3): (methyl) phospholipids, fatty acids
~ 2870-2830	ν_s (CH_2): (methylene) phospholipids, long chain fatty acids
~ 1739-1713	ν (C=O): phospholipids, cholesterol esters, glycerides
~ 1713-1589 ~ 1654	ν (C=O): proteins, lipids amide I
~ 1589-1474 ~1545	δ (N–H): proteins, lipids amide II
~1480-1430	δ_{as} (CH_3), δ_{as} (CH_2), δ_s (CH_3), δ_s (CH_2): phospholipids, fatty acids, glycerides
~1420-1370	ν (COO^-): (carboxylate ions) amino-acids
~1280-1220	ν (P=O): (phosphate) phospholipids
~1300-900	ν (C–O): saccharides, glucose, lactate

ν = stretching vibrations (s = symetric, as = asymetric), δ = bending (scissoring) vibrations

For further analysis only the spectral region 1710 – 900 cm^{-1} known as "fingerprints" spectral region was taken into account. Within the fingerprints region there are some characteristic bands attributed to proteins, lipids, carbohydrates and nucleic acids. Nine main absorption massifs were identified in this region. The first is attributed to amide I and its maximum absorption value are at around ~1643 cm^{-1} for normal tissue and ~ 1650 $cm^{-1}$for adenoma and carcinoma samples. The maximum value of absorption within the amide II massif is at around 1537 cm^{-1} for all studied tissue types. Within the region between 1476-1350 cm^{-1} there are many bands attributed to the lipids, proteins, fatty acids and amino acids which can overlap. Nevertheless there were observed two absorption maxima for all cases at around 1454 cm^{-1} and 1394 cm^{-1}. Then there are visible bands of rather small absorption value with the maximum at 1315 cm^{-1} for normal tissue and at 1309 cm^{-1} for adenoma and carcinoma. They are probably connected with proteins. There is also clearband connected with PO_2^-asymmetric stretch assigned to DNA observed at 1237 cm^{-1} for all

analysed tissue types. The next absorption area located between 1180 and 1140 $cm^{-1}$is varied for the studied cases and the maximum absorption values fall at 1160 cm^{-1} for normal tissue, 1169 cm^{-1} for adenoma, and at 1155 cm^{-1} for carcinoma. The last broad absorption mass if between 1135-980 cm^{-1}isattributed mainly to carbohydrates and nucleic acids. The most striking difference between analysed tissue types is seen exactly within this region. There is a markedly increased absorption for carcinoma samples especially at two main absorption peaks at around 1080 cm^{-1} and 1038 cm^{-1}. The first is assigned to symmetric PO_2^-band while the second is connected with glycogen. In the case of normal and adenoma tissues, those absorption bands are not so clearly outlined, but rather a broad hump, without a clearly defined maximum, are seen.

Figure 2 shows the fingerprints region with enlarged amide I spectral range of averaged spectra of studied tissue types. The differences in the position of the dominant absorption band are seen. To analyse that alteration the second derivative spectra were used to reveal the main absorption bands within the 1700-1600 cm^{-1} spectral range. The minimum values on second derivative spectra within the amide I region were at: ~ 1695 cm^{-1}, ~1682 cm^{-1}, ~1668 cm^{-1}, ~1659 cm^{-1}, ~1651 cm^{-1}, ~1645 cm^{-1}, ~1637 cm^{-1}, ~1628 cm^{-1}, ~1619 cm^{-1}. Every individual absorption band is associated with a specific secondary structure of proteins. Three absorption bands – 1695, 1682 and 1628 cm^{-1} were assigned to the β-sheet protein structure, bands at 1668 and 1619 cm^{-1} were connected with β-turns while the bands at around 1659 and 1651 cm^{-1} were attributed to α-helix. There was also observed unordered structure connected with 1645 cm^{-1} as well as triple helix at around 1637 cm^{-1} [22]. The presented absorption bands have an approximate character as the minimum values of second-derivative for each individual spectrum oscillated around the given values. To determine the content of individual protein secondary structures in studied tissue types the area under the second derivatives was analysed for every single spectra. The results are shown in Figure 3. There are two ways of presentation. One is based on relative values of proper secondary protein structures (Fig.3A). The relative content was determined as the percentage of a given structure in relation to the total amide I area understood as the sum of all absorption bands within those area. The second presentation shows absolute values obtained from the analysis (Fig.3B).

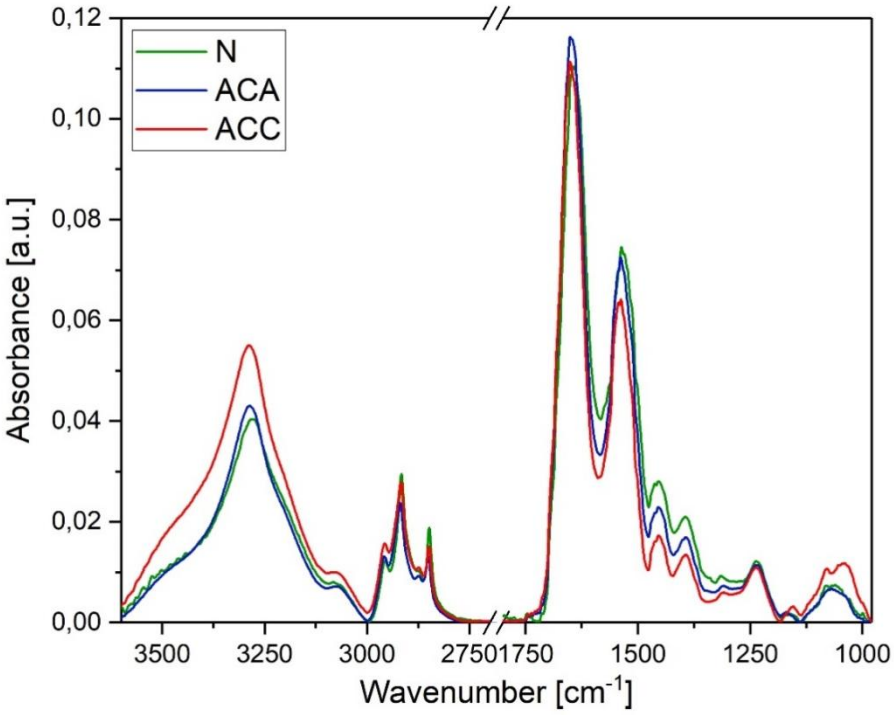

Figure 1: Comparison of averaged spectra for normal adrenal cortex (N), adrenal cortical adenoma (ACA) and adrenal cortical carcinoma (ACC) for whole measured spectral range.

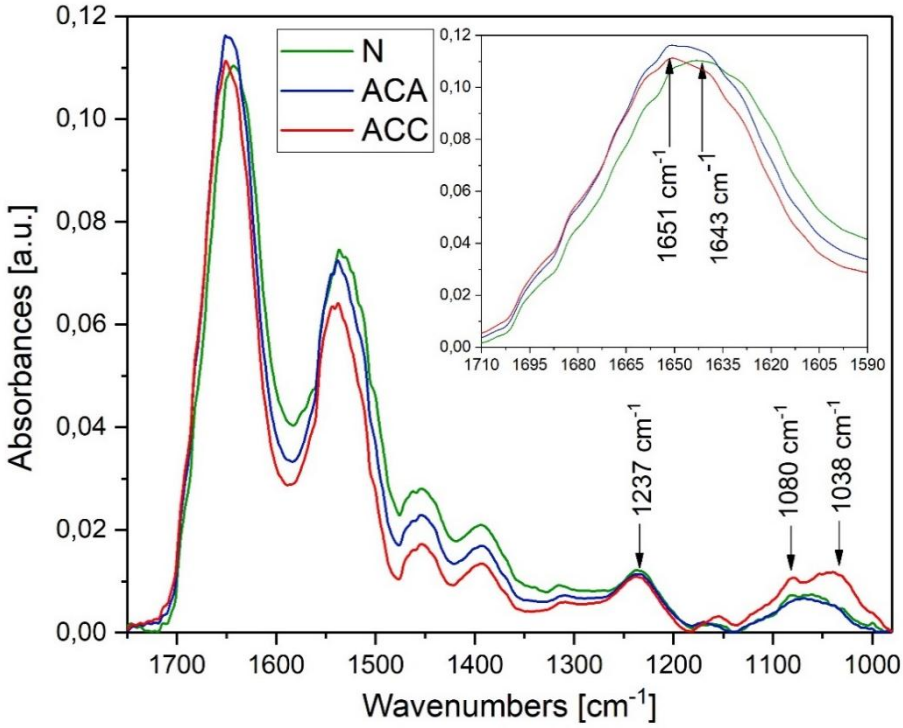

Figure 2: Comparison of averaged spectra for normal adrenal cortex (N), adrenal cortical adenoma (ACA) and adrenal cortical carcinoma (ACC) for whole measured the fingerprints spectral range. The inset shows the enlarged amide I region.

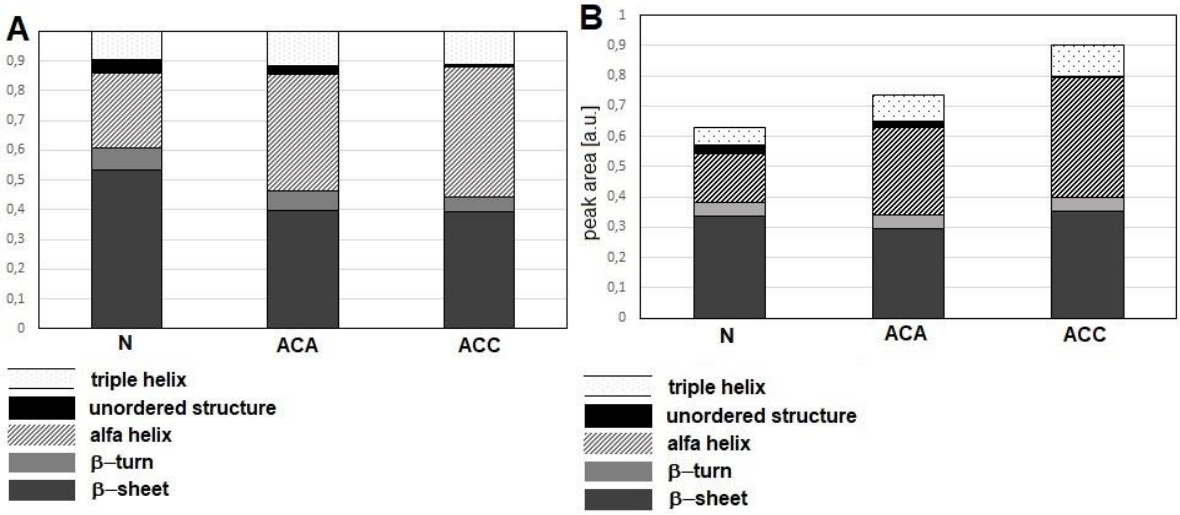

Figure 3: The presentation of secondary protein structure content in studied tissue types: A) percentage values B) absolute values.

The non-parametric U-Mann Whitney test was applied to find out if there are any differences between the analysed tissue samples concerning the particular secondary protein structures. The results are shown in table 3 for both absolute and relative (percentage) values.

Table 2: Results of Mann-Whitney U-test for comparison of the secondary protein structures among analysed groups

Absolute values	α-helix	β-sheet	β-turn	Unordered structure	Triple helix
N ↔ ACA	-	+	-	+	+
N ↔ ACC	+	-	-	+	+
ACA ↔ ACC	+	+	-	-	-
Percentage values					
N ↔ ACA	-	+	-	+	+
N ↔ ACC	+	+	+	+	+
ACA ↔ ACC	-	-	+	-	-

"+" means significant differences between groups with p<0, 05, while "-" means the lack of differences between groups.

It is seen that the statistical outcomes of analysis depend on the approach and they differ for absolute and relative content of particular protein structures.

In presented study we also analysed the areas of chosen absorption massifs within the fingerprints region. The outcomes were obtained from pre-processed (as described earlier) spectra for studied tissue samples. We measured both: the areas around the maximum absorption bands as well as the chosen ratios of the areas of absorption bands. The measurement of relative contents minimizes the impact of any differences in the thickness of the samples.

The most frequently the analysed absorption bands are related to the amide I massif being regarded as a specific "internal standard". This is justified when the amide I content is constant and comparable for all samples tested. In the case of the presented results, the better parameter that served as the "internal standard" was the massif under the peak at around 1454 cm^{-1}. It turned out that the area of the absorption band of 1454 cm^{-1} is comparable for all studied tissue types and does not show any statistically significant differences between samples.

Table 3 shows the statistically significant differences between analysed parameters. Figure 4 shows the median, minimal and maximal values of IR absorption bands and ratios of absorption bands of analysed biochemical parameters for all three studied groups.

Table 3: Results of Mann-Whitney U-test for comparisons of the analysed groups performed for chosen biochemical parameters

	N ↔ ACA	N ↔ ACC	ACA ↔ ACC
spectral ranges around the maximum absorption bands			
Amid I	+	-	-
Amid II	+	-	+
1454 cm-1	-	-	-
1394 cm-1	+	+	-
1237 cm-1	-	+	-
Carbohydrates	-	+	+
Ratios of spectral ranges			
Amide I/1454 cm-1	-	-	-
Amide II/1454 cm-1	+	-	+
1237/1454 cm-1	+	+	-
Carbohydrates /1454 cm-1	-	+	+

"+" means significant differences between groups with p<0, 05, while "-" means the lack of differences between groups.

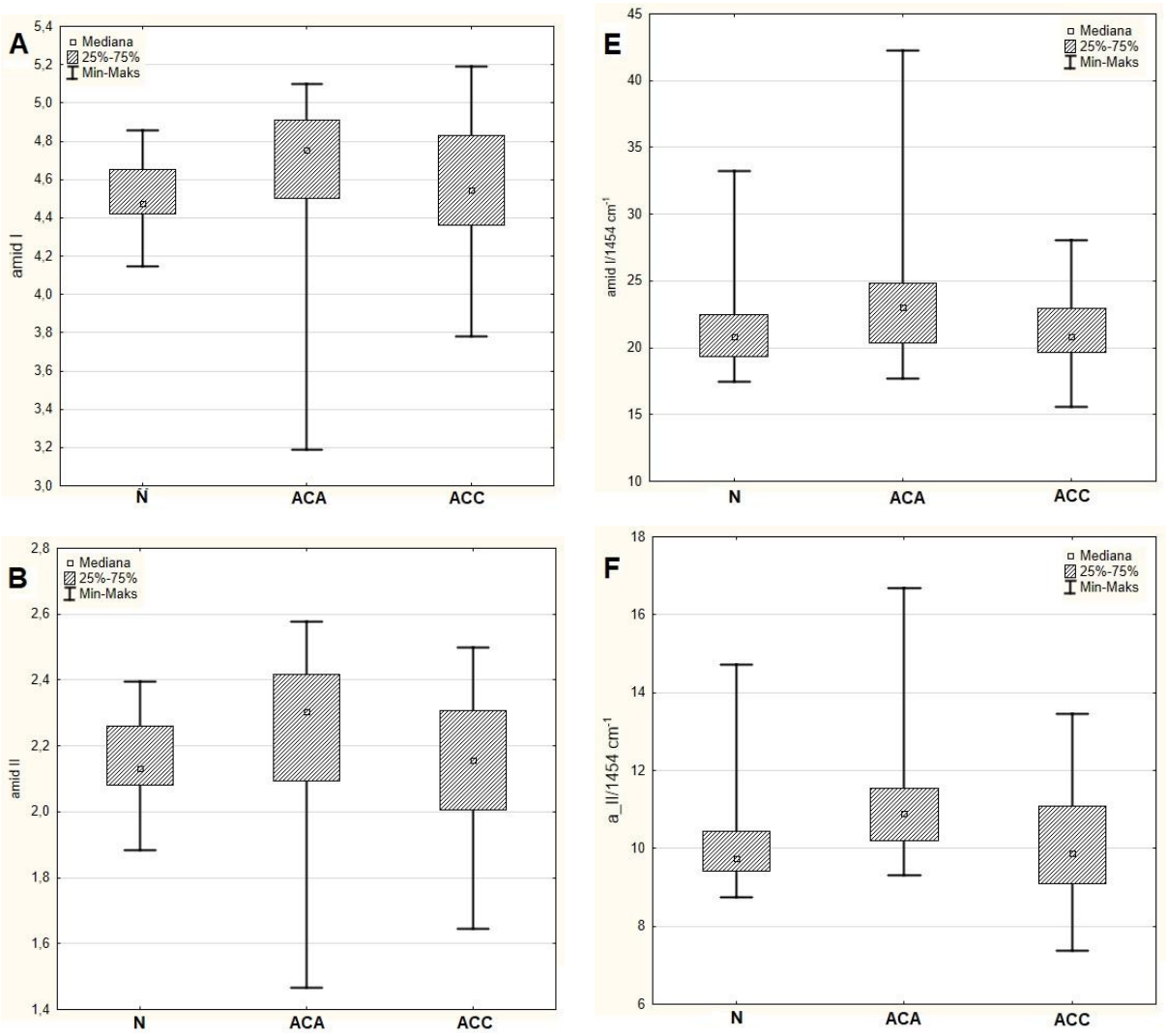

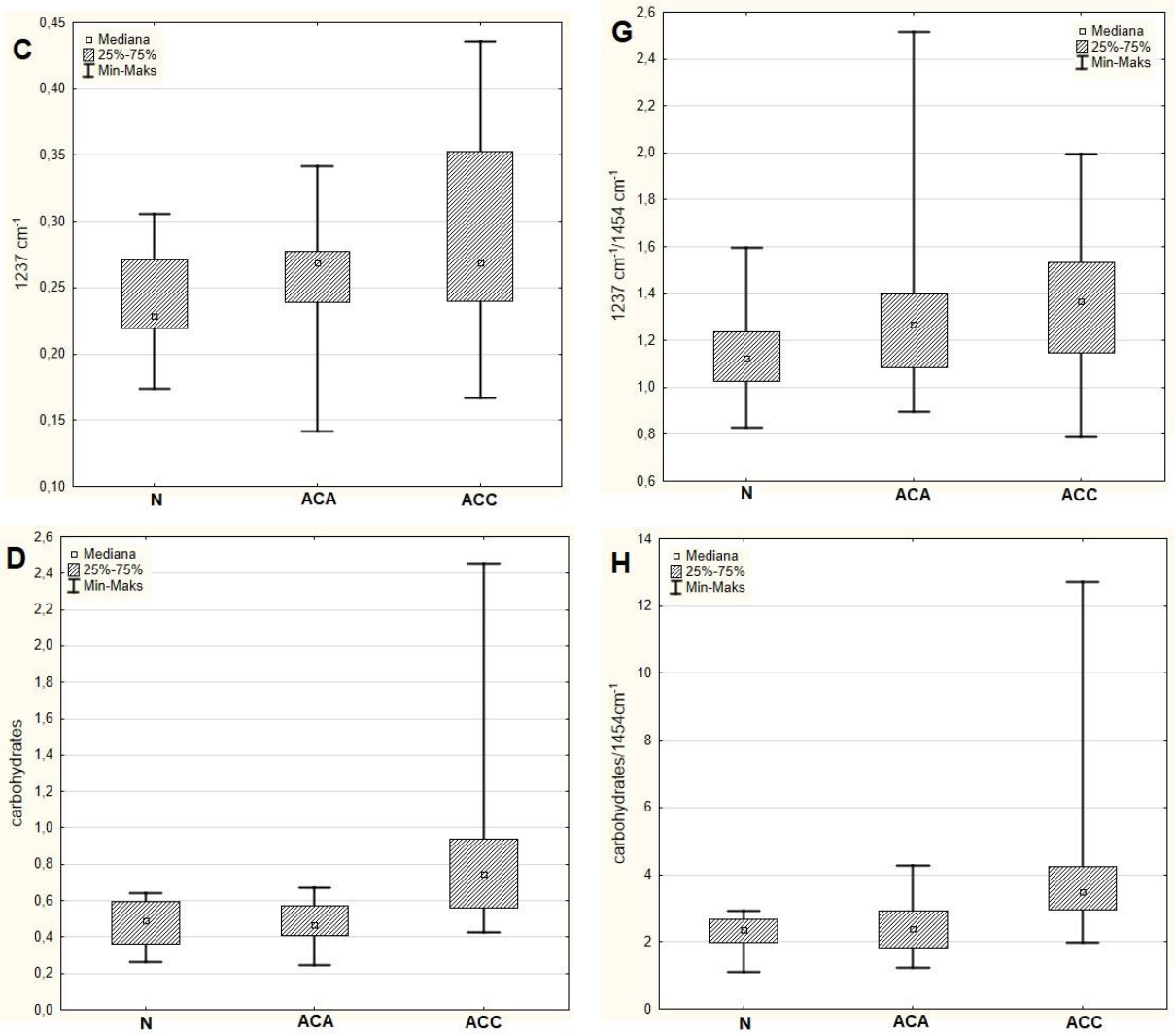

Figure 4: The median, minimal and maximal values of biochemical parameters presenting differences between normal adrenal cortex (N), adrenocortical adenoma (ACA) and adrenocortical carcinoma (ACC) groups. The figures A-D present the net value of absorption of chosen biochemical parameters while the figures E-H presents the absorption ratios of that parameters.

4. Discussion

In our analysis we focused only on the spectral region 1710 – 900 cm^{-1} known as "fingerprints" spectral region. The reason of such procedure was that the measured tissue samples derived from paraffin–embedded tissue blocks. As a paraffin mask the molecular composition of samples, it was removed by xylene during dewaxing protocol. Nevertheless there is still probability that traces of paraffin may remain in the samples and interfere with the signal from native tissue components [23, 24, 25]. The paraffin-related absorption bands are at around 1462, 2846 and 2954 cm^{-1}. To avoid potential impact of paraffin residues those bands were excluded from the analysis. Hence it was decided that the analysis of the fat massif (between 3000 and 2830 cm-1) would be abandoned. One should perceive that the xylen could affect the lipid structures and in consequence it could impact on the tissue lipid content [26]. Our observations revealed also that the shape of spectra within the lipid massif obtained from dewaxed tissues is different than those for fresh tissues. The absorption bands are thinner and clearly separated while in fresh derived tissue samples spectra the absorption of the lipid massif is extremely high and the bands are merged [27].

From the results presented in table 3 it is seen that relative content of amide I is the same for all-normal cortex (N), adrenocortical adenoma (ACA) and adrenocortical carcinoma (ACC). In case of amide II massif it was noticed that there are statistically significant differences between N and ACA tissue samples as well as between ACA and ACC tissue samples. The area of massif around the 1237 cm^{-1} is statistically lower for N than for ACA and ACC (Fig.4C). This absorption band is commonly attributed to DNA content hence the elevated value in adenoma and carcinoma might indicate increased proliferation in those samples. This parameter should be compared to the RNA content. It is assumed that the band of RNA is located at around 1123 cm^{-1}. In presented study it was not possible to clearly determine the content of the RNA due to scattering and diffraction effects within considered spectral range. Nevertheless it seems that in pathological tissues there is a tendency for faster proliferation. In case of carcinoma it is additionally confirmed by the microscopic view of histological sample.

The tissue cells in adrenocortical carcinoma are smaller, not uniform and with visibly irregular structure of cell nuclei. It is well known that rapidly multiplying cells show a greater demand for energy and thus for carbohydrates. The results are in line with this fact. Adrenocortical carcinoma tissue samples show statistically higher amount of carbohydrates in general comparing to normal and adrenocortical adenoma samples (Fig.4D). This is the most striking difference among studied tissue types.

As far as the location of absorption bands are taken into account, there is no observable evidence of differences between tissue types. The only contrast is visible within the amide I region but in fact it concerns the position of the most intense absorption bands but not a shift of them (because the second derivative analysis showed that the absorption bands are the same for studied samples).

5. Conclusion

The presented results show that it is possible to compare IR spectra of the deparaffinised samples from adrenal gland tissues but the differences are not so evident. The only spectral region which could be taken into differentiation procedure is connected with absorption band attributed to DNA (1237 cm^{-1}) and the whole massif related mainly with carbohydrates between 1130 and 980 cm^{-1}. Based on the measurements which were carried out and comparing with the results obtained for fresh tissues [27], it can be assumed that the preparation of the samples has a significant impact on the results. Perhaps it would be a good idea to investigate how the procedure of the samples deparaffinising might influences the results. It is worth to investigate the other deparaffinising protocolto find out if the results will be the same. In our opinion it is a good direction to use the archival tissue samples to find out some biomolecular indicators of pathological changes, especially under the circumstances of such rare diseases as adrenocortical carcinoma is. The studies have preliminary character and should be continued.

Acknowledgements

The authors declare no conflicts of interest. This work was supported by the Polish Ministry of Science and Higher Education and its grants for Scientific Research.

References

[1] Lack, E. E. Tumors of the Adrenal Glands and Extraadrenal Paraganglia, AFIP Atlas of Tumor Pathology, series 4; ARP Press Silver Spring: Maryland (2007) 1-35, 57-124, 241-274.
[2] T. Bednarczuk, M. Bolanowski, K. Sworczyk et al., Adrenal incidentaloma in adults – management recommendations by the Polish Society of Endocrinology, Polish Journal of Endocrinology 67 (2) (2016) 234-258.
[3] M. Terzolo, A. Stigliano, I. Chiodini et al., AME Position Statement on adrenal incidentaloma, European Journal of Endocrinology 164 (2011) 851-870.
[4] S. Aubert, A. Wacrenier, X. Leroy et al., Weiss system revisited: a clinicopathologic and
[5] immunohistochemical study of 49 adrenocortical tumors, Am. J. Surg. Pathol., 26 (12) (2002) 1612-
[6] 1619.
[7] L. Thompson, Pheochromocytoma of the Adrenal gland Scaled Score (PASS) to separate benign from
[8] malignant neoplasm: a clinicopathologic and immunophenotypic study of 100 cases, Am J Sur Pathol 26 (2002) 551-566.
[9] S. G. Creemers, L. J. Hofland, E. Korpershoek et al., Future directions in the diagnosis and medical treatment of adrenocortical carcinoma, Endocrine-Related Cancer 23 (2016) R43-R69, DOI: 10.1530/ERC-15-0452.
[10] T. J. Giordano, Classification of adrenal cortical tumors: Promise of the ‘molecular’approach, Best Practice & Research Clinical Endocrinology & Metabolism 24 (2010) 887-892, DOI: 10.1016/j. beem.2010.10.012.
[11] M. Walsh, M. German, M. Singh et al., IR microspectroscopy: potential applications in cervical cancer screening, Cancer Lett.246 (2007) 1-11.
[12] K. Das, C. Kendall, I. Martin et al., FTIR of touch imprint cytology: A novel tissue diagnostic technique, J. Photoch. Photobiol. B: Biol.92 (2008) 160-164.
[13] H. Fabian, P. Lasch, M. Boese, W. Haensch, Infrared microspectroscopic imaging of bening breast tumor tissue sections, J. Mol. Struct.661-662 (2003) 411-417.
[14] M. A. Mackanos, C. H. Contag, FTIR microspectroscopy for improved prostate cancer diagnosis, Trends Biotechnol.27 (2009) 661-663.
[15] D. Townsend, M. Milijković, B. Bird et al., Infrared micro-spectroscopy for cytopathological classification of esophageal cells, Analyst 140 (2015) 2215-2223.
[16] O. J. Old, L. M. Fullwood, R. Scott et al., Vibrational spectroscopy for cancer diagnostics, Analytical Methods 6 (2014) 3901-3917, DOI: 10.1039/c3ay42235f.
[17] D. Simonova, I. Karamancheva, Application of Fourier Transform Infrared Spectroscopy for Tumor Diagnosis, Medical Biotechnology 27 (6) (2013) 4200-4207.
[18] V. Zohdi, D. R. Whelan et al., Importance of Tissue Preparation Methods in FTIR Micro-Spectroscopical Analysis of Biological Tissues: ‘Traps for New Users’, PLoS ONE 10 (2) (2015) 1-11, doi: 10.1371/journal. pone.0116491.
[19] M. J. Baker, J. Trevisan, P. Bassan et al., Using Fourier transform IR spectroscopy to analyse biological materials, Nature Protocols 9 (8) (2014) 1771-1791.
[20] Optical Spectroscopy and Computational Methods in Biology and Medicine (series: Challenges and Advances in Computational Chemistry and Physics, vol 14), edited by Małgorzata Barańska, Springer, Dordrecht 2014.

[21] K. R. Bambery, B. R. Wood and D. McNaughton, Resonant Mie Scattering (RMieS) correction applied to FTIR images of biological tissue samples, Analyst 137 (2012) 126-132.
[22] K. Wehbe, J. Filik, M. D. Frogley, G. Cinque, The effect of optical substrates on micro-FTIR analysis of single mammalian cells, Analytical and Bioanalytical Chemistry 405 (4) (2013) 1311-1324.
[23] C. Petibois, G. Déléris, Evidence that erythrocytes are highly susceptible to exercise oxidative stress: FT-IR spectrometric studies at the molecular level, Cell Biol Int 29 (2005) 709-716.
[24] C. Petibois, G. Déléris, Erythrocyte adaptation to oxidative stress in endurance training, Arch Med Res 36 (2005) 524-531.
[25] K. Wehbe, R. Pinneau et al., FT-IR spectral imaging of blood vessels reveals protein secondary structure deviations induced by tumor growth, Analytical and Bioanalytical Chemistry 392 (2008) 129-135.
[26] J. Rieppo, R. Rieppo, S. Saarakkala and J. S. Jurvelin, in Fourier Transforms – New Analytical Approaches and FTIR Strategies, ed. G. S. Nikoloc, InTech (2011) 3-14.
[27] M. Verdonck, N. Wald, J. Janssis et al., Breast cancer and melanoma cell line identification by FTIR imaging after formalin-fixation and paraffin-embedding, Analyst 138 (2013) 4083-4091.
[28] C. Hugher, L. Gaunt, M. Brown et al., Assesment of paraffin removal from prostate FFPE section using transmission mode FTIR-FPA imaging, Analytical Methods 6 (2014) 1028-1035.
[29] J. Surmacki, B. Brozek-Pluska, R. Kordek, H. Abramczyk, The lipid-reactive oxygen species phenotype of breast cancer. Raman spectroscopy and mapping, PCA and PLSDA for invasive ductal carcinoma and invasive lobular carcinoma, Molecular tumorigenic mechanisms beyond Warburg effect, Analyst 140 (2015) 2121–2133, http: //dx. doi. org/10.1039/c4an01876a.
[30] J. Dudala, M. Bialas, et al., Biomolecular characterization of adrenal gland tumors by means of SR-FTIR, Analyst 140 (2015) 2101-2106.